Effects of electron–vibration coupling in transport through single molecules

2012 J. Phys.: Condens. Matter 24 394002

(http://iopscience.iop.org/0953-8984/24/39/394002)

IOP PUBLISHING JOURNAL OF PHYSICS: CONDENSED MATTER
J. Phys.: Condens. Matter **24** (2012) 394002 (15pp) doi:10.1088/0953-8984/24/39/394002

TOPICAL REVIEW

Effects of electron–vibration coupling in transport through single molecules

Katharina J Franke and Jose Ignacio Pascual

Fachbereich Physik, Freie Universität Berlin, Arnimallee 14, 14195 Berlin, Germany

E-mail: franke@physik.fu-berlin.de

Received 15 January 2012, in final form 1 March 2012
Published 11 September 2012
Online at stacks.iop.org/JPhysCM/24/394002

Abstract
Using scanning tunneling spectroscopy, we study the transport of electrons through C_{60} molecules on different metal surfaces. When electrons tunnel through a molecule, they may excite molecular vibrations. A fingerprint of these processes is a characteristic sub-structure in the differential conductance spectra of the molecular junction reflecting the onset of vibrational excitation. Although the intensity of these processes is generally weak, they become more important as the resonant character of the transport mechanism increases. The detection of single vibrational levels crucially depends on the energy level alignment and lifetimes of excited states. In the limit of large current densities, resonant electron–vibration coupling leads to an energy accumulation in the molecule, which eventually leads to its decomposition. With our experiments on C_{60} we are able to depict a molecular scale picture of how electrons interact with the vibrational degrees of freedom of single molecules in different transport regimes. This understanding helps in the development of stable molecular devices, which may also carry a switchable functionality.

(Some figures may appear in colour only in the online journal)

Contents

1. Introduction

The ultimate goal of molecular electronics is to replace inorganic semiconductor technology by cheap and versatile molecular materials. The basic components of molecular electronic circuits are custom-synthesized molecules acting as diodes, transistors or switches contacted to two electrodes and exposed to an externally controlled bias voltage. Chemical synthesis routes seem to offer any desirable molecular property and functionality. However, the electronic coupling of the molecule to the electrodes drastically modifies the free molecule properties. Design strategies for electronic circuits thus need to consider the molecule and the contacts as a complex entity rather than only the individual molecule.

The electronic conductance of a molecule contacted to a metallic electrode is characterized by the electronic structure of the molecule and the electronic coupling to the electrodes. The hybridization of the molecular states with the electronic bands of the electrodes leads to a shift and broadening of the formerly discrete states and determines the electronic conductance properties. Additionally, the electron transmission is affected by the coupling of the electrons to molecular vibrations [1]. The excitation of molecular vibrations may proceed resonantly or non-resonantly, depending on the energy level alignment and the applied voltage. Non-resonant electron–vibration coupling plays a role when the highest occupied molecular orbital (HOMO) and the lowest unoccupied molecular orbital (LUMO) derived resonances lie far outside the transport window and the tunneling electron inelastically scatters at the molecule, exciting molecular vibrations [2, 3]. This leads to a change of conductance due to the opening of an additional transport channel, reflected as steps in the dI/dV spectra. In the case of resonant electron transport, the inelastic tunneling proceeds in the molecular ionic state [4]. The corresponding vibronic states act as resonant transmission channels giving rise to peaks in the dI/dV–V spectra. To be able to resolve these states, the lifetime broadening of the molecular resonances has to be smaller than the energy separation of the vibrational states. With typical vibrational energies of the order of ≈100 meV, the lifetime of the electronically excited state should exceed 10 fs. This is only achievable if the molecules are not in direct contact with a metal substrate but decoupled by an isolating layer [4, 5].

Besides changes in the transmittivity of the molecular junction, electron–vibration coupling may crucially affect the junction stability. When the energy stored in the molecular vibrations exceeds a critical limit, the molecule dissociates. The limit of molecular degradation by electronic currents is thus an important parameter for potential applications. If a typical single molecule with a contact resistance of 10–100 kΩ is biased by 1 V, the current reaches 10–100 μA. This corresponds to an electron transmission rate of 10^{13}–10^{14} s^{-1}. Typically, vibrations relax by the excitation of electron–hole pairs in the metal surface in a ps timescale [6]. Despite these fast relaxation rates and only small vibrational excitation probabilities of 0.1–1%, the balance between the rates of vibrational excitations and energy dissipation leads to an efficient accumulation of energy in the molecule, eventually resulting in its degradation.

While the fast energy damping into the leads is advantageous for the stability of a molecule, it also hinders particular applications, such as switching processes. Usually, isomerization events require longer lifetimes than the extremely short lifetimes of excited states of molecules in contact with a metal electrode [7]. Hence, their quantum yield is reduced by several orders of magnitude or even fully suppressed [7–9]. The engineering of molecule–metal contacts thus needs to balance considerations of functionality and stability.

In this overview, we aim to capture the basic mechanisms and effects of electrons exciting molecular vibrations in single molecules in view of the molecular conductance and stability. The C_{60} molecule embedded in different surroundings has proved to be an ideal playground for exploring different transport regimes by tunneling spectroscopy. We first discuss the probability of exciting certain vibrational modes and their detection capabilities in the non-resonant tunneling regime in section 4. In section 5, we describe the requirements and strategies for detecting fingerprints of resonant electron–vibration coupling. In the limit of large current densities, the resonant vibrational excitation eventually even leads to the dissociation of the C_{60} molecules. We explore this limit in section 6 and show how the balance between energy generation and dissipation at the molecule–metal junction can be tuned to increase the molecular stability [10, 11].

2. Experimental method

We used scanning tunneling microscopy (STM) and spectroscopy (STS) to probe electron-induced vibrational excitations in C_{60}. The spatial resolution of STM allowed us to characterize the adsorption configuration and to measure the transport of electrons through the molecules at specific molecular sites. The experiments were carried out in a custom-made ultra-high vacuum (UHV) STM running at a base temperature of 4.8 K. C_{60} molecules were deposited on different low index surfaces of metal single crystal surfaces, which had been cleaned under UHV conditions by several cycles of Ne^+ ion sputtering followed by thermal annealing. The resulting surfaces probed with the STM showed atomically flat terraces with a very low density of defects and impurities. Indentations of the STM tip into the substrate were used regularly to ensure a good coating of the tip with the material of the substrate. Different substrates were chosen with different electronic properties, to change the energy level alignment of the C_{60} resonances with respect to the Fermi level (E_F).

3. Adsorption properties of C_{60} on metal surfaces

The fullerene C_{60} is a well suited candidate to study electron–vibration coupling by tunneling spectroscopy. Due to its three-dimensional shape (figure 1), the adsorption on metal surfaces is expected to hardly influence the intrinsic molecular properties. In particular, the molecular orbitals and vibrational modes remain almost unperturbed. The 46 vibrational states of the icosahedral cage can be classified into ten different point group symmetries [12]. The vibrational activity of C_{60} has been widely studied by optical techniques: due to symmetry selection rules, only the $T1_u$ modes are infrared active, while the A_g breathing modes and H_g modes have been observed in Raman spectroscopy [13]. The set of H_g modes arises from the deformation of the molecule upon electron attachment into the threefold degenerate LUMO orbital. They are hence Jahn–Teller (JT) active. The JT-active modes of C_{60} have also been detected in photoemission [14] and electroluminescence [15]. A few of these vibrations have been identified in resonant transport experiments when the

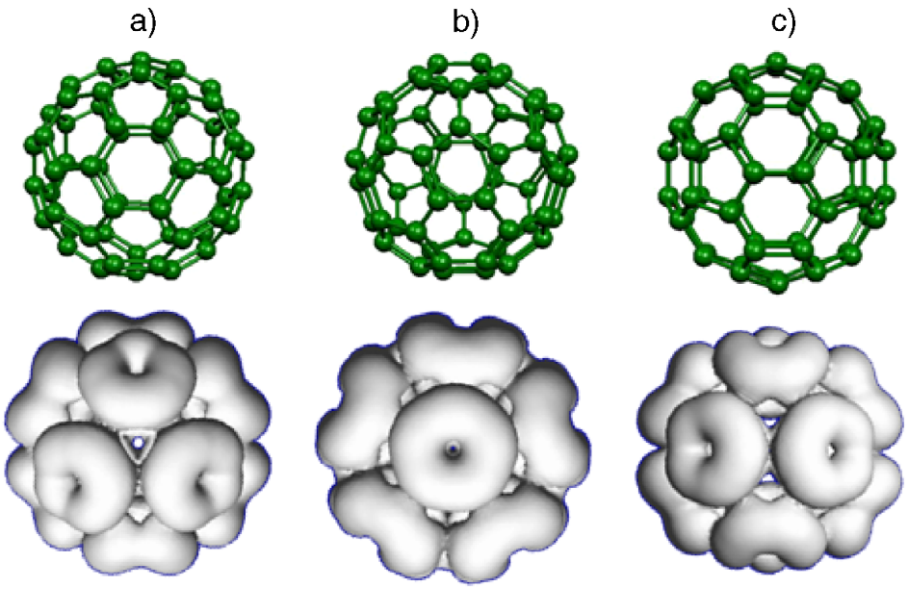

Figure 1. Molecular structure of a C_{60} molecule. When the molecule is adsorbed on a surface, there are three outstanding high-symmetry orientations. The molecule may expose (a) a hexagon on top, (b) a pentagon on top, or (c) a C–C double bond on top. The LUMO isosurface is mainly located on the carbon pentagons, giving rise to the typical symmetries seen in STM images for the three orientations (compare figure 2).

molecules are weakly interacting with the substrate [5, 16]. In the non-resonant limit, only very weak vibrational activity has been observed [5, 17–20].

STM images of C_{60} molecules adsorbed on Cu(110), Pb(111), and Au(111) surfaces are shown in figure 2. On all these substrates, C_{60} nucleates in ordered islands when the substrate is kept close to (or above) room temperature during deposition. The intramolecular resolution resembles the LUMO shape in figure 1, indicating an almost unperturbed molecular orbital structure on metal surfaces [21–26]. One can further infer the orientation of the fullerene cage (compare to figure 1). On the Cu(110) surface, the fullerenes adsorb between four of the topmost copper atoms, keeping a pentagon–hexagon C–C bond pointing upwards [27]. On Pb(111) only few of the molecules show intramolecular contrast (figure 2(b)), while most of them appear featureless and thus indicate similar adsorption states [28]. C_{60} islands on Au(111) evidence a large variety of molecular orientations [25], as one can determine from the intramolecular structure resembling the lobed shape of the LUMO resonance [21].

The molecular resonance structure of C_{60} on these metal surfaces is probed by tunneling spectroscopy (STS) and shown in figure 3. At positive sample bias, each peak corresponds to a resonant electron channel through an unoccupied molecular state of the fullerene (LUMO and LUMO + 1). On Cu(110), the LUMO is a broad peak at ∼0.2 V and is partially occupied. On Pb(111), the LUMO alignment lies close to this value. However, its sharper lineshape revealed by the corresponding peak (apparently split in figure 3(b)) shows only a small tail crossing the Fermi level E_F, indicating a smaller amount of charge transfer into the C_{60}. A negligible charge transfer for C_{60} on Au(111) can be deduced from the far alignment of the LUMO derived peak with respect to E_F, at ∼0.8 eV [21, 29]. A second resonance associated to the LUMO + 1 is also observed in all the STS spectra. The HOMO is found as a broad shoulder at negative sample bias. As we will show later, the molecular resonance alignment is crucial for the efficiency of exciting molecular vibrations, i.e. resonant versus non-resonant electron–vibration coupling in the investigated transport energy window.

4. Inelastic tunneling spectroscopy of C_{60}: off-resonance electron–vibration coupling

The idea of inelastic tunneling spectroscopy (IETS) in an STM junction is based on early experiments on tunneling junctions formed by thin molecular layers enclosed between two metal plate electrodes [30]. The tunneling barrier and conductance properties are sketched in figure 4. A small fraction of the electrons passing through a molecule are scattered inelastically. This inelastic process can essentially be regarded as a non-resonant tunneling mechanism, in which the tunneling electron loses energy by exciting a molecular vibration. The energy loss process opens a new transport channel, thus leading to a step-wise increase in the differential conductance at the threshold of vibrational excitation ($\hbar\omega$). Typically, the efficiency of the inelastic excitation is very small, leading to changes of conductance of the order of a few per cent. Experimentally, it is easier to detect the corresponding features in the d^2I/dV^2–V spectra, in which the dI/dV steps are reflected as peaks/dips at positive/negative bias voltage (figure 4(b)).

The IETS technique has been put forward as a sensor for the chemical identity of single molecules, since the vibrational fingerprint is unique to the chemical bonds in the molecule [2, 3, 31]. One drawback, however, is that so far only a relatively small number of molecules have

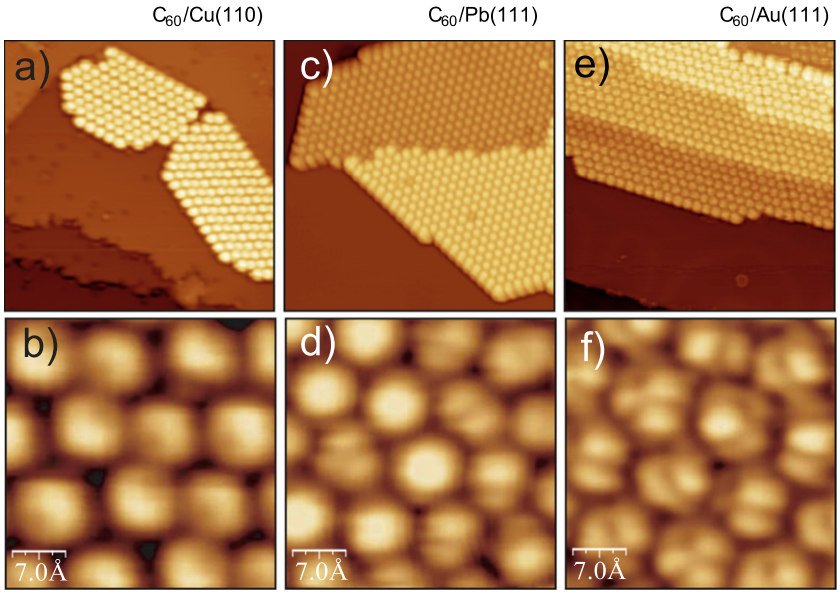

Figure 2. Large scale STM images and zoomed regions enhancing the intramolecular resolution of C_{60} monolayer islands grown on ((a), (b)) Cu(110), ((c), (d)) Pb(111) and ((e), (f)) Au(111). In all cases, the STM images were obtained with positive sample bias, hence corresponding to the unoccupied density of states. In this way, the lobed structure observed in some molecules can be identified with the spatial shape of unoccupied orbitals. Reproduced with permission from [108]. Copyright 2011 Pan Stanford Publishing.

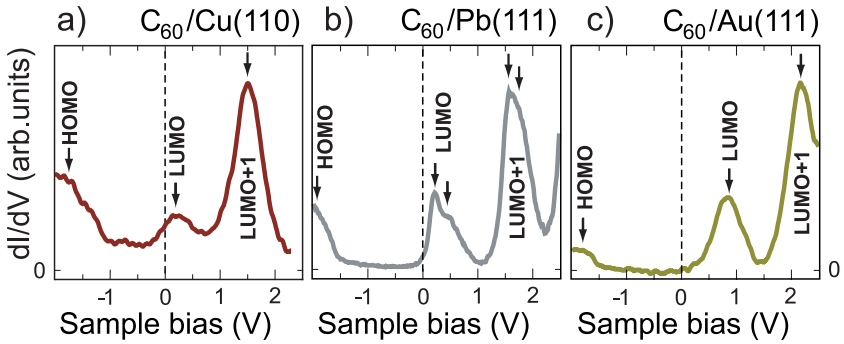

Figure 3. Differential conductance spectra of C_{60} on the different surfaces shown in figure 2. Arrows mark the fitted positions of HOMO, LUMO and LUMO + 1. The spectra were measured by positioning the STM tip on top of a single molecule and ramping the bias voltage V while keeping the tip–molecule distance constant (feedback loop open). Arrows identify the molecular states. dI/dV data were obtained by using a lock-in amplifier with an rms modulation amplitude V_{ac}. (Cu: $R_{junct} = 1.1$ GΩ, $V_{ac} = 20$ mV; Pb: $R_{junct} = 0.7$ GΩ, $V_{ac} = 5$ mV; Au: $R_{junct} = 0.3$ GΩ, $V_{ac} = 30$ mV.) Reproduced with permission from [108]. Copyright 2011 Pan Stanford Publishing.

shown inelastic features in STM. The absence of any sizable signals for many molecular species questions the general applicability of this technique. Furthermore, selection rules, as are well known for optical spectroscopic techniques, are still elusive. Instead, a set of propensity rules has been suggested theoretically [32–35]. Their experimental verification is ongoing. Using C_{60} molecular junctions as an example, we show that the interaction between the molecule and the surface plays a crucial role in the detection mechanism. Furthermore, symmetry rules based on electron–vibration coupling apply in certain transport regimes.

It should be noted that inelastic tunneling can not only be used as a chemical probe, but the selective excitation of vibrations offers an appealing procedure to induce molecular motion, dissociation and isomerization [36–43].

4.1. Inelastic tunneling spectra of C_{60}

The inelastic tunneling spectra of C_{60} molecules strongly depend on the surface. We first explore inelastic tunneling spectra of the fullerene on a Pb(111) substrate. A typical d^2I/dV^2–V spectrum taken on a single molecule embedded in the hexagonal monolayer is depicted in figure 5(a). It shows nine pairs of peaks and dips in the window of 200 meV at positive and negative bias voltages, respectively, on top of a broad background. The background has most weight at 150 meV, which is associated to the largest slope in the tail of the LUMO derived resonance at 200 meV (compare to figure 3(b)).

To get a quantitative insight into the strength of the vibrational excitations, we subtract the background and normalize the spectrum by the corresponding differential

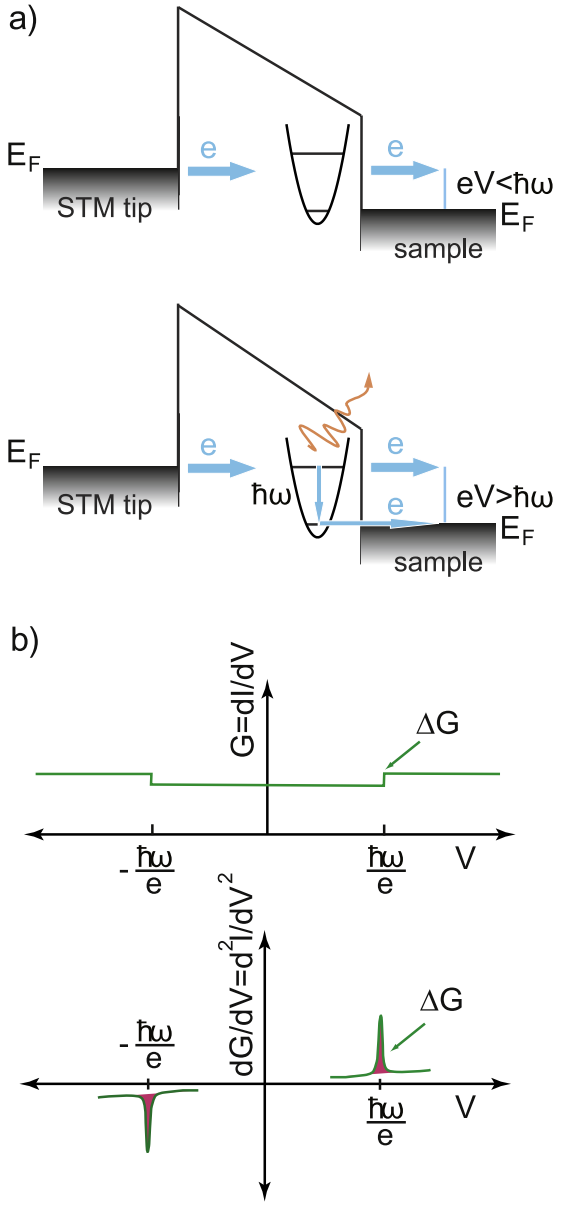

Figure 4. (a) Model potential tunneling barrier with a molecule placed in the barrier. The molecular vibrations are represented as a simple harmonic oscillator. When the energy of the tunneling electrons is below any molecular excitation they can only tunnel elastically. When the electron energy exceeds the energy threshold for molecular excitation an additional tunneling path is opened, where the electrons tunnel inelastically off the molecule. (b) The effect of the inelastic channels is ideally a small step-wise increase in the differential tunneling conductance ($\mathrm{d}I/\mathrm{d}V$–V). This induces a peak in the $\mathrm{d}^2I/\mathrm{d}V^2$–$V$ spectrum.

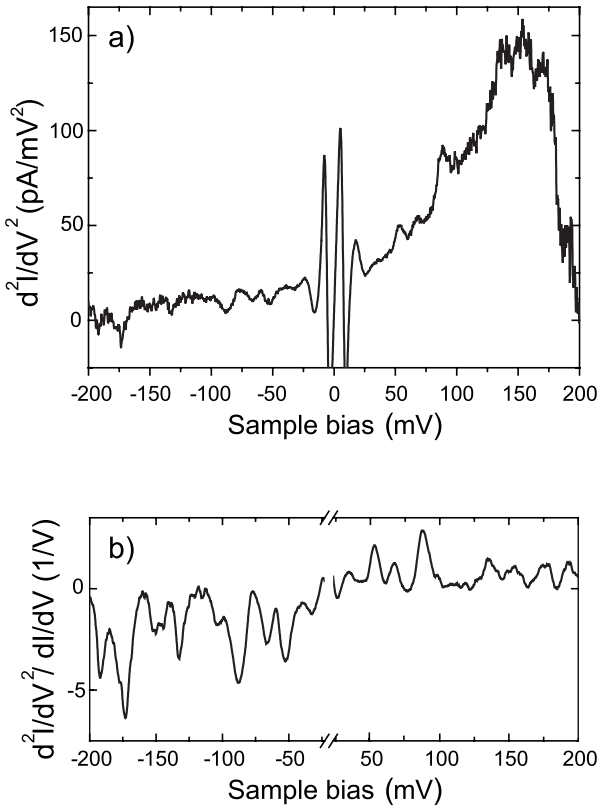

Figure 5. (a) A typical $\mathrm{d}^2I/\mathrm{d}V^2$–$V$ spectrum in the tunneling regime (junction conductance $\approx 0.03G_0$) of C_{60} on Pb(111) shows nine peaks at positive sample bias and nine dips at the equivalent negative sample bias on top of a broad background. The background is due to the LUMO resonance. The strong peaks around E_F are due to the superconducting gap at 4.5 K of the Pb(111) substrate and have been omitted for clarity in the following figures. The spectrum is recorded as the second harmonic signal by the lock-in technique ($f_{mod} = 723$ Hz, $U_{mod} = 6$ mV_{rms}). (b) After background subtraction and normalization by the corresponding $\mathrm{d}I/\mathrm{d}V$–V spectrum, the peak/dip pairs become more evident.

conductance of the junction, i.e. by the simultaneously acquired $\mathrm{d}I/\mathrm{d}V$–V spectrum. The resulting spectrum, shown in figure 5(b), clearly displays antisymmetric peaks at equivalent positive/negative sample bias. They correspond to the opening of new tunneling channels at the threshold energy, at which electrons excite molecular vibrations. The finding of nine excitations exceeds the limited observation of only a few modes in other IETS experiments, where C_{60} was in contact with different metal electrodes [5, 17–20]. This system thus allows a detailed analysis of the excitation and detection mechanism of molecular vibrations in electron transport.

4.1.1. Excitation of Jahn–Teller active modes. We first aim to identify the nine observed modes (out of the 46 possible vibrations) [44]. Figure 6 shows a high resolution $\mathrm{d}^2I/\mathrm{d}V^2$–$V$ spectrum at negative sample bias. Table 1 summarizes the observed eigenenergies and their corresponding changes in conductance. Comparison to the eigenmodes of a free C_{60} molecule yields that the set of eight H_g vibrations nicely matches the inelastic excitations in our $\mathrm{d}^2I/\mathrm{d}V^2$–$V$ spectra (see the dashed lines in figure 6). The clear observation of the complete set of H_g modes calls for selection rules in IETS. Conceptually, the selected excitation of H_g modes is easy to understand. The electron transport in this energy window is mediated by the tail of the LUMO resonance both above and below the Fermi energy (indicated by the shaded area in figure 7(a)). Hence, at both bias polarities, the transient tunneling through the LUMO resonance causes Jahn–Teller-like deformations of the icosahedral cage, which are described by the set of H_g vibrational modes [12, 45].

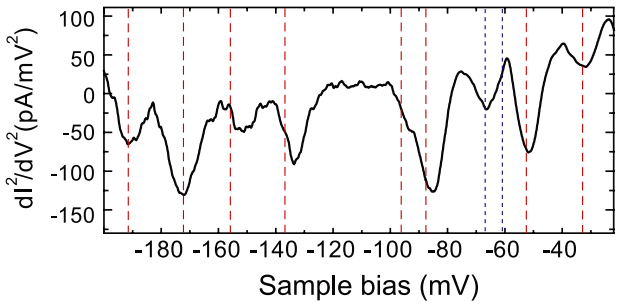

Figure 6. d^2I/dV^2–V spectrum of C_{60} on Pb(111) after background subtraction and normalization by dI/dV, zoomed at negative sample bias. The red dashed lines indicate the energies of the eight H_g modes of a free C_{60} molecule. The blue dashed lines indicate the A_g mode at 62 meV and the $T1_u(1)$ mode at 67 mV [13]. Adapted with permission from [44]. Copyright 2010 American Chemical Society.

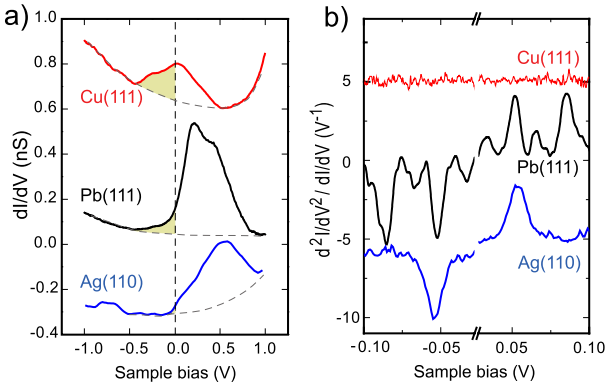

Figure 7. (a) Differential conductance spectra of C_{60} on Cu(111), Pb(111), and Ag(110) (opening feedback loop at $U_b = 2.0$ V, $I_t = 1.2$ nA; $U_b = 2.0$ V, $I_t = 1$ nA; $U_b = 0.5$ V, $I_t = 0.4$ nA, for Cu, Pb, Ag, respectively, $U_{mod} = 10$ mV_{rms}). The broad peaks correspond to the LUMO derived resonance of C_{60}, appearing with different degrees of Fermi level crossing (shadowed areas). The dashed line indicates the background. (b) Normalized and background subtracted inelastic tunneling spectra of C_{60} on the same three metal surfaces as in (a). For the data on Cu(111), we test the appropriate experimental conditions by detecting small inelastic signals of vibrational features in the IETS spectra of co-adsorbed CO molecules. Adapted with permission from [44]. Copyright 2010 American Chemical Society.

The assignment of the peak at 67 mV is ambiguous because it lies in an energy region with various vibrational modes. Since the A_g modes (at 62 and 184 meV) are also known to have considerable electron–vibration coupling with the LUMO, we may tentatively assign the 67 mV peak to the $A_g(1)$ vibration [16]. However, we cannot exclude that this excitation corresponds to the $T1_u(1)$ mode. Its activation would agree with partial charge transfer and a small intrinsic distortion of the icosahedral cage on the surface [12, 46].

While these observations underline the importance of selection rules in IETS, we note that this experiment on C_{60} is characterized by a peculiar energy level alignment. Even though the transport regime is non-resonant, as the LUMO is located outside the vibrational band of C_{60}, the influence of the molecular resonance in the tunneling is appreciable. This seems to strengthen excitation mechanisms, like those expected in the resonant limit. In experiments with different

Table 1. Table of vibrational modes detected in the IETS spectra with their symmetry and change of conductance.

$\hbar\omega_\nu$ (meV)	Mode ν	$\frac{\Delta G}{G}$ (%)
34 ± 2	$H_g(1)$	1.4
52 ± 2	$H_g(2)$	5.2
67 ± 2	$A_g(1)$ or $T1_u(1)$	2.2
87 ± 2	$H_g(3)$	5.6
97 ± 3	$H_g(4)$	1.6
137 ± 2	$H_g(5)$	3.5
155 ± 2	$H_g(6)$	2.1
175 ± 2	$H_g(7)$	6.7
196 ± 2	$H_g(8)$	3.1

energy level alignments or mixing of orbitals at E_F, this selection may not be appropriate. IETS experiments, e.g., on self-assembled molecular monolayers, primarily reveal infrared, i.e. dipole active, modes [47]. Earlier theoretical works have pointed out the role of the symmetry of the molecular states close to the Fermi level E_F [32, 48]. It is thus more appropriate to claim propensity rules instead of selection rules in transport experiments [34].

4.1.2. The role of energy level alignment on the detection of molecular vibrations of C_{60}. The observation of nine modes of C_{60} adsorbed on Pb(111) is remarkable when compared to results on other metal substrates [5, 17–20]. One peculiarity of the Pb substrate is that it is superconducting at the temperature of our measurements (4.5 K). However, we find no evidence of an enhancement of the inelastic signal due to the corresponding quasi-particle density of states, when we compare IETS spectra below and above the critical superconducting temperature ($T_c = 7.2$ K). The excitation of H_g modes in the d^2I/dV^2–V spectra on Pb(111) already indicates the importance of the LUMO tail in the transport experiment. Therefore, we turn to a comparison of the molecular density of states at E_F and the vibrational activity on different surfaces.

Submonolayer coverages of C_{60} on Ag(110) and Cu(111) are arranged in densely packed hexagonal islands. On Ag(110), the LUMO resonance is found at ~0.5 eV [17], with very little overlap with E_F (figure 7(a)). The corresponding d^2I/dV^2–V spectrum reveals only the $H_g(2)$ mode. A weaker vibrational activity thus coincides with a smaller LUMO weight at E_F than on Pb(111). This tendency is further followed by the absence of any IETS signal when the LUMO is even further away from E_F, as, e.g., on Au(111). This is in line with our arguments from above; the existence of molecular states around E_F enhances the inelastic excitation process [48].

One may hence expect the largest inelastic features when the LUMO resonance is very close to E_F. Such an energy level alignment can be found for C_{60} on Cu(111). The resonance appears split into two peaks. One of them is located in the negative bias region (figure 7(a)). However, the corresponding d^2I/dV^2–V spectrum is completely featureless. Since the sensitivity to such small signals in STM relies on excellent experimental conditions, we simultaneously test our system on co-adsorbed CO molecules. With the same experimental

conditions resolving frustrated translation and rotation modes of CO in the d^2I/dV^2–V spectra, the vibrational fingerprint on C_{60} is absent.

The surprising disappearance of inelastic fingerprints on C_{60} on Cu(111) thus requires a more elaborate picture of the complete transport process, in which the detection of vibrations is suppressed. It is known that the proximity of molecular resonances to E_F also enhances second order (vibration emission and absorption) processes, which can partly annihilate the effect of the inelastic channels [48–50] and may even cause a peak-to-dip inversion in the lineshape of some modes [51]. Although this effect could lead to a substantial decrease of the inelastic signal, it can hardly explain by itself a completely featureless spectrum like in figure 7(b).

One important aspect of the LUMO being located in the same energy window as that in which we probe the vibrations is the change from off-resonance to on-resonance electron transport through the C_{60} molecule. In this case vibrational states of the molecular ion are accessible for resonant electron tunneling (see also section 5). For molecular species electronically decoupled from the metal surface, these resonant vibrational excitations appear as peaks in the vibrational spectra. Here, the fullerenes are in direct contact with the Cu surface, causing molecular vibrations to be quickly damped by excitation of electron–hole pairs in the metal substrate [11, 52]. The vibrational signal then broadens and simply contributes to an overall widening of the conductance spectra, rather than appearing as narrow peaks.

The detection of molecular vibrations in transport thus requires a delicate balance between a resonant enhancement of the vibrational activity and charge fluctuations at the interface suppressing the signal. Charge fluctuations probably play a particularly important role in the excitation of vibrational modes intrinsically coupled with the emptying or filling of charge into the molecule, as is the case for Jahn–Teller active modes. It should also be noted that charge fluctuations may also cause other types of vibrational excitations, such as, e.g., dipole active modes [47]. It is thus not surprising that many molecule–surface systems do not easily show clear selection rules or provide the perfect requirements for the observation of any inelastic excitations.

4.1.3. IETS: from tunneling to the contact regime. The increase of conductance by opening of an additional transport channel at the threshold for inelastic excitation is symptomatic for tunneling processes. Electron transport through quantum point contacts shows the opposite behavior: inelastic scattering processes lead to a reduction of conductance. In the limit of a perfectly transmitting state, i.e. with transmission probability of an incoming electron to the opposite electrode with $\tau = 1$, any electron which loses energy by inelastically scattering at a molecular vibration is forbidden from traveling further across the junction, since all the forward momentum states are occupied. Hence, the momentum needs to be reversed, thus resulting in enhanced backward scattering and reduced forward transport. Consequently, vibrational excitations reduce the conductivity

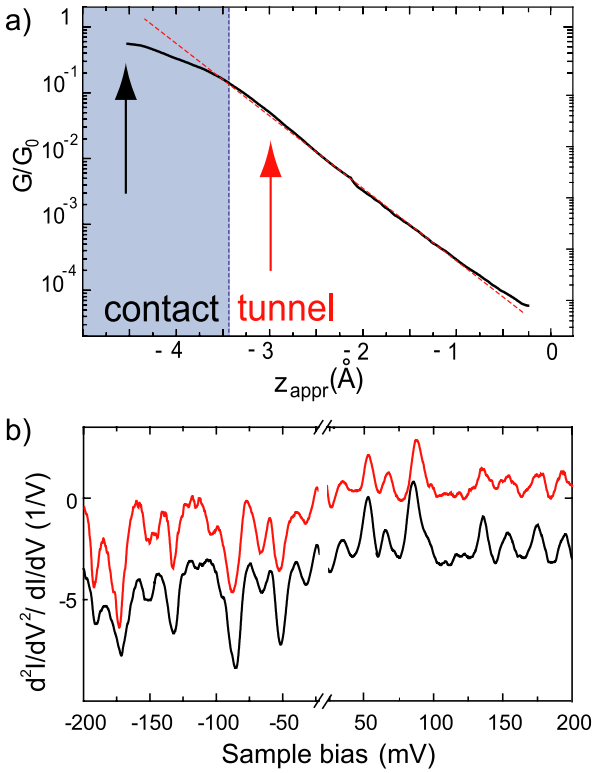

Figure 8. (a) Increase of the junction conductance G as the tip is approached a distance z_{appr} toward a C_{60} molecule ($U_b = 400$ mV and $I_t = 1.2$ nA initially). (b) d^2I/dV^2–V spectra at two different tip–molecule distances (marked by arrows in (a)) representing the tunnel and contact regimes with corresponding junction conductances of $0.03G_0$ and $0.25G_0$, respectively. For a direct comparison of the spectra, the background arising from the LUMO resonance, which broadens upon tip contact, has been subtracted. Subsequent normalization by their differential conductance dI/dV–V leads to the d^2I/dV^2–V spectra shown. The spectrum at $0.25G_0$ has been offset for clarity.

through the molecule [53–55]. This is represented as dips in the corresponding d^2I/dV^2–V spectra instead of peaks.

In STS, we can measure inelastic excitation spectra at any arbitrary value of the junction conductance, allowing us to explore the range from tunneling to the contact regime. During the approach of the tip toward a C_{60} molecule on Pb(111), the tunneling current I–z_{appr} increases exponentially, in agreement with the reduction of the tunneling barrier height. At a junction conductivity of ~7.5 μS, the current smoothly levels off to a flatter I–z_{appr} behavior (figure 8(a)). We ascribe this region to a mechanical tip–C_{60} contact [10, 56]. This junction conductance is much smaller than G_0, the conductance of a fully transmitting channel (G_0: quantum of conductance, $G_0 = \frac{2e^2}{h} = 77.5$ μS), as governed by Landauer theory and describing the transport through atomic contacts [57, 58]. Furthermore, in a C_{60} junction the regime from tunneling to contact occurs in a broad range of tip positions. This is due to fast bistable fluctuations of the fullerene between the tip and the sample due to an effective heating of the molecular junction [10, 56, 59].

To compare the inelastic excitation spectra of C_{60} in different transport regimes, we approach the STM tip 3 Å and

4.5 Å toward the fullerene, to reach junction conductances of $0.03G_0$ and $0.25G_0$, respectively. Comparison with the approach curves of figure 8(a) indicates that these junction conductance values correspond to the tunnel and contact regimes. The two d^2I/dV^2–V spectra in figure 8(b) are consecutively taken on the same molecule. After normalization of both spectra by their differential conductances, the same nine vibrational modes can be observed with similar intensities and lineshapes. At first sight, this seems to contradict the prediction of a peak-to-dip inversion of the d^2I/dV^2–V spectra when crossing the transition between the tunnel and contact regimes. However, our contact regime is characterized by a very small contact conductance. This implies that there are still empty forward momentum states, which allow for a preferred forward scattering as opposed to backward scattering. A transition between preferential forward and backward scattering has been found at a conductance of $0.5G_0$ per transmission channel [34, 55]. Thus, the low contact conductance found for C_{60} on Pb(111) dictates that this system behaves still as a tunnel junction with inelastic excitations leading to an increased molecular conductance. We further note that there is no observable shift of the molecular eigenmodes from the tunneling to the contact regime, as has been reported for small molecules, which suffer a considerable deformation by the presence of the STM tip [60].

5. Resonant electron–vibration coupling

In section 4.1.2 we have shown, with the example of C_{60} on Pb(111), that the resonant character of the tunneling due to the overlap of the LUMO tail with E_F can enhance the electron–vibration coupling. Contrary to expectations, in the resonant limit, as has been achieved for C_{60} on Cu(111), the IETS spectra do not show any clear features. A simplified picture of the molecular energy levels when C_{60} is in direct contact with a metal surface is shown in figure 9(a). Due to a significant overlap of the molecular states with the substrate states, the molecular derived resonances are broadened substantially. The attachment of an electron into this resonance has a very short lifetime due to the fast decay of the electron into the substrate. The transient lifetime (τ) scales inversely with the width of the resonance (Γ) ($\Gamma\tau \approx \hbar$) [31]. Hence, vibronic states are hidden in the overall lineshape of the dI/dV–V spectra [61]. Consequently, it is impossible to disentangle effects of electron–vibration coupling. In order to gain access to resonant vibronic states, the lifetime broadening needs to be smaller than the energy separation of the vibrations (see figure 9(b)). Only in this case can resonant electron–vibration coupling be detected as peaks in the dI/dV–V spectra above the LUMO resonance [5, 16]. The intensities of the peaks are ruled by Franck–Condon transitions from the ground state to the transient anionic state.

5.1. Self-assembled decoupling layers

A strategy to enlarge the excited state lifetimes is to reduce the electronic coupling with the metallic substrate

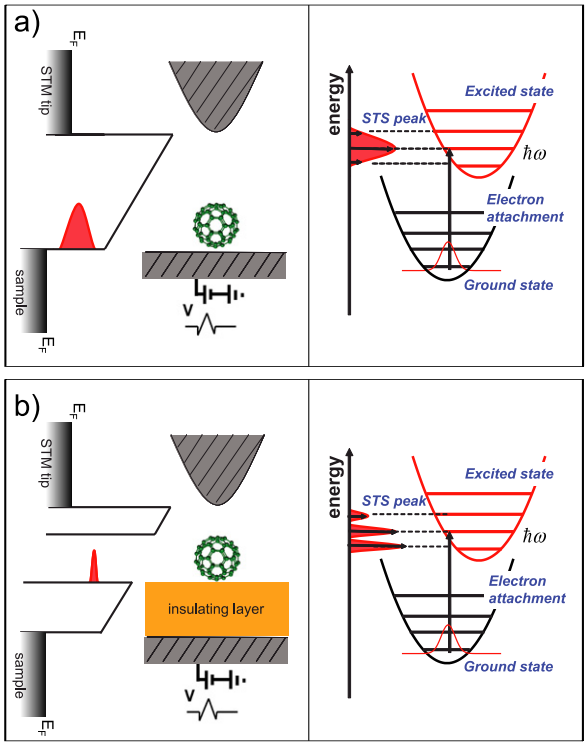

Figure 9. (a) When a molecule is adsorbed directly on a metal surface, the molecular orbital derived resonances are broadened due to hybridization with the substrate. The lifetimes of electronically excited states are extremely short. Any possible vibrational states are hidden in the broad lineshape of the molecular resonances. (b) A thin insulating layer decouples the electronic states of the molecule from the substrate. This results in narrower molecular resonances and longer lifetimes of excited states. When the resulting resonance width is smaller than the vibrational energies, vibronic states can be detected as separate peaks in the dI/dV–V spectra.

by introducing dielectric spacers, which are thin enough to allow charge injection. Ultra-thin films of oxides [62–64], ionic salts [15, 61, 65], nitride [66, 67] or alkanethiol layers [68, 69] have been used to successfully decrease the electronic overlap between atomic or molecular states and the metal substrate. The photoluminescence of decoupled C_{60} molecules has shown a full set of Jahn–Teller active modes [15]. Electron transport through C_{60} on thin alumina films revealed sharpened molecular resonances, but only a few molecular vibronic states [16, 70]. On the other hand, from section 4.1.1, we see that the complete set of H_g modes couples efficiently to tunneling electrons. One may thus expect a fingerprint of all these modes in the resonant transport experiment, when C_{60} is sufficiently decoupled from the surface [71].

A common aspect to most decoupling layers used so far is that they are thin films of bulk isolator materials. We have explored an alternative approach for decoupling C_{60} molecules based on the self-assembly of organic molecules. The mixture of C_{60} and 1,3,5,7-tetraphenyladamantane (TPA) on Au(111) leads to ordered nanostructures, in which the fullerene is lifted from the surface by means of lateral non-covalent interactions with TPA molecules [72, 73]. One of the observed structural

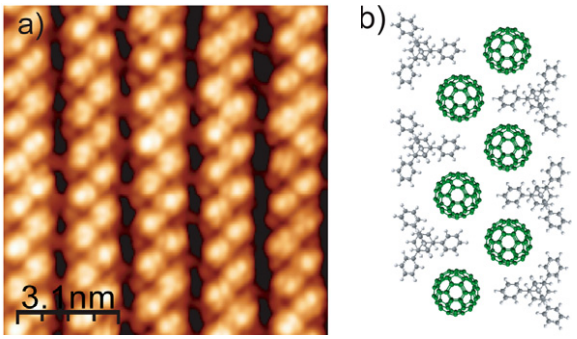

Figure 10. (a) STM image after deposition of C_{60} onto a Au(111) surface, which has been pre-covered with 0.9 monolayers of tetraphenyladamantane (TPA) ($I = 18$ pA, $V = 820$ mV). Clearly observable are double rows of alternating TPA and C_{60} molecules. (b) Corresponding structural model. For STM image processing we used the free software WSxM [107].

motifs is double rows of alternating TPA and C_{60} (figure 10). The neighboring insulating rows can function as troughs for further C_{60} molecules, as, e.g., the one shown in figures 11(a) and (b).

Current–voltage (I–V) and differential conductance ($\mathrm{d}I/\mathrm{d}V$–V) spectra taken over the center of these fullerenes reveal a large HOMO–LUMO gap of ∼3.4 eV accompanied by strong non-linearities around −2.0 V, 1.4 V and 2.2 V, associated with the HOMO, LUMO and LUMO + 1 derived resonances, respectively (figure 11(c)). Both the wide gap compared to the HOMO–LUMO energy distance of a neutral C_{60} molecule (∼1.8 eV) and the sharp resonance states are clear fingerprints of a molecule which interacts weakly with its surroundings [73]. The timescale of the transient ionic state populated during tunneling can be estimated from the width of the LUMO resonance. The LUMO's FWHM is ∼60 meV, corresponding to a tunneling lifetime of ∼10 fs. This value determines the energy resolution of the vibrational excitations, being now closer to the characteristic energy scale of the energy difference between modes.

5.2. Vibronic states in decoupled C_{60} molecules

Instead of a discrete set of peaks above the LUMO resonance of C_{60} on this template, due to individual vibrational excitations, we find a broad satellite at a distance of ∼230 meV above the LUMO resonance. This energy alignment is unexpected, since the vibrational band of C_{60} is only 200 meV wide. However, in photoemission experiments on free C_{60} molecules, a vibronic peak ascribed to the Jahn–Teller effect has been identified at 230 meV above the LUMO [14]. This comparison suggests that electron transport through the fullerenes in the troughs of the organic template does indeed show effects of electron–vibration coupling.

A detailed computational analysis of electron–vibration coupling provides an explanation of the appearance of a peak outside of the vibrational energy band. Frederiksen *et al* used density functional theory to calculate the electron–vibration coupling strength upon attachment of an electron into the LUMO resonance [71]. Similarly to the observations in

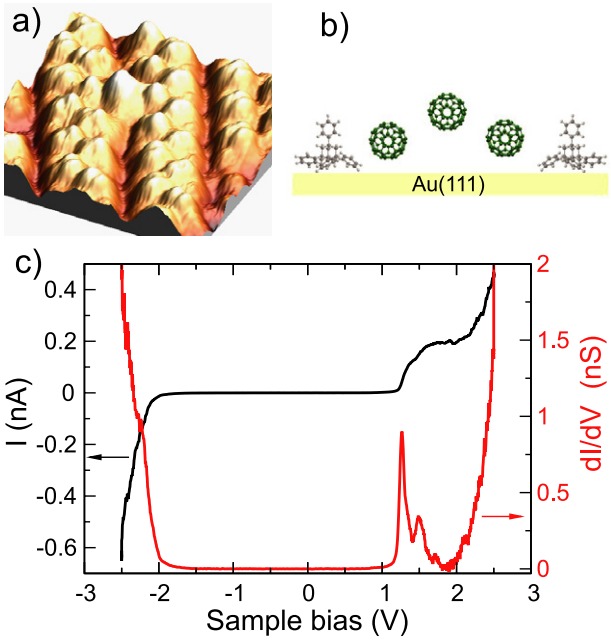

Figure 11. (a) Pseudo-three-dimensional representation of an STM image of the double rows of alternating TPA/C_{60} on the Au(111) surface ($I = 16$ pA, $V = 580$ mV). Some isolated C_{60} molecules are adsorbed in the troughs between the rows and are thus much higher. (b) Side view of the structural model along the supporting line of C_{60} in the troughs, evidencing the increased distance to the Au(111) substrate. (c) $\mathrm{d}I/\mathrm{d}V$–V spectrum recorded on top of such a fullerene (feedback opened at $I = 0.46$ nA, $V = 2.5$ V, modulation amplitude $V_{\mathrm{rms}} = 14$ mV).

section 4, only the Jahn–Teller active modes play a role in the transport experiment. One important result of the simulations is that at the timescale of the tunneling processes quantum fluctuations among equivalent deformations according to the dynamic JT effect take place. These cause the excitation of multiple JT vibrational states, and their respective overtones. Convolution of the theoretically derived vibronic states with the width obtained from our experiments results in a shoulder reproducing our experimental results (blue spectrum in figure 12). This agreement between theory and experiment corroborates that the peak is a fingerprint of resonant electron–vibration coupling in a single C_{60} molecule in transport, despite the absence of discrete vibronic states in the spectra.

6. Effects of electron–vibration coupling at larger current densities

The experiments shown above clearly indicate that the inelastic scattering of tunneling electrons to excite C_{60} modes is an effective way to deposit energy into the molecular vibrational states of a molecule. At typical tunneling currents, the excitation does not usually lead to a detectable effect on the molecule. The rate of inelastic scattering (the inelastic fraction) is considerably smaller than the rate at which excited vibrations of molecules on surfaces decay (typically of the order of $1/(10\,\mathrm{ps})$ or higher). Hence, in the low current regime the molecule is essentially 'vibrationally' cold.

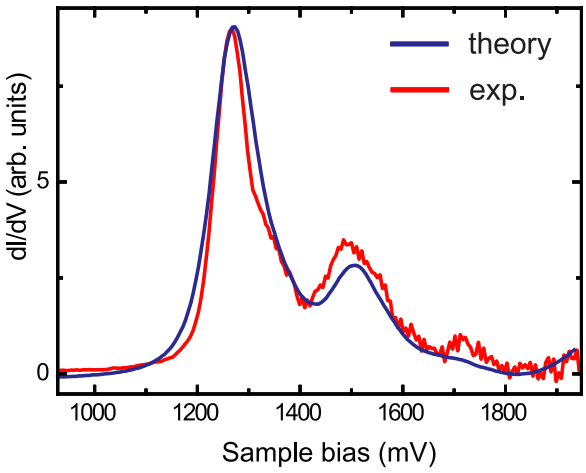

Figure 12. The experimental dI/dV–V spectrum on a decoupled C_{60} molecule (red line) reveals clear satellites at distances of ∼230 and ∼460 meV above the LUMO resonance. The theoretical spectrum (blue line) was computed by coupling the LUMO to the JT-active A_g and H_g modes of C_{60}. To reproduce the experimental peak widths a broadening of 60 meV has been introduced into the calculations [71].

In the high-current regime, the average time between molecular excitations can become smaller than the timescale of vibrational quenching. In this case, multiple excitation of molecular vibrations leads to an efficient accumulation of energy in the molecule. The stored energy can be regarded as the effective temperature of the molecular junction [10, 11, 56, 74–77]. A common definition relates the energy of the non-equilibrium excitation of molecular vibrations in transport to the equilibrium Bose–Einstein distribution with the same integrated energy. The corresponding temperature defines the temperature of a single molecule [10, 74, 75].

Several previous studies estimated the temperature of single molecules contacted to an STM or AFM tip [10, 11, 56, 76, 77]. They found a striking dependence of the molecular temperature on the applied bias voltage, indicating the roles of different transport mechanisms. From these experiments an (indirect) estimation of the temperature has been deduced, amounting to several hundred degrees for currents of a few μA. For most organic molecules, these temperatures are of the order of their thermal degradation temperatures. These observations show that molecular devices would practically operate close to the limit of their stability [78]. Thus, for the implementation of molecules as active components of electronic devices, a thorough understanding of heat generation, i.e. efficient excitation of molecular vibrations, and heat dissipation, i.e. quenching of molecular vibrations, is indispensable. The following sections elucidate the limit of molecular degradation by excitation of vibrations in a single molecule.

6.1. Vibration-induced molecular dissociation

We first describe experiments carried out on a single molecule adsorbed on a Cu(110) surface. Its structure and molecular resonance alignment have already been described in section 3. In order to explore the regime of large tunneling currents

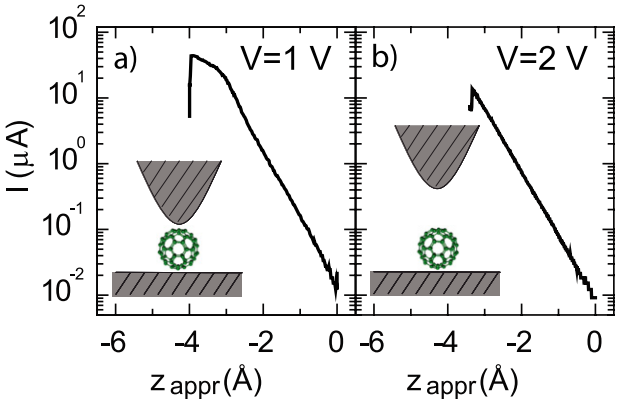

Figure 13. Current versus tip approach plots for C_{60} molecules on Cu(110) showing a sharp jump associated to molecular decomposition (a) after forming a tip–C_{60} contact ($V = 1.0$ V, acquisition time $t = 1.5$ s) and (b) in the tunnel regime ($V = 2.0$ V).

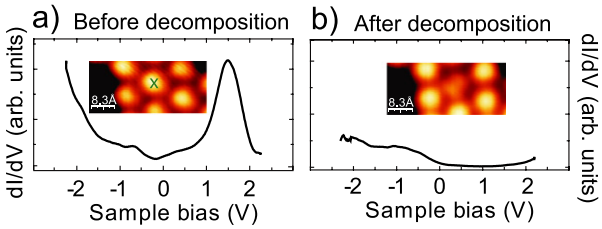

Figure 14. (a), (b) STS spectra of C_{60} on Cu(110) before and after an $I(z_{appr})$ plot like in figure 13, respectively. The disappearance of the molecular resonance structure in (b) reveals the decomposition of the molecule by the large current density. The insets show STM images of the molecular island before and after tip indentation at the marked point. The molecule underneath the tip has an apparent lower height. Adapted with permission from [10]. Copyright 2008 American Physical Society.

flowing through a C_{60} molecule, the STM tip is placed on top of a selected fullerene and approached a distance z_{appr}, keeping the sample bias constant.

If a small positive sample bias is maintained ($V < 0.6$ V) the tunneling current ($I(z_{appr})$) shows a similar increase to the one shown previously in figure 8(a); the molecule stays unaffected after bringing the tip into mechanical contact and further indentation for several ångstroms. In this case, the tunneling current can reach up to 100 μA [10, 26, 56, 59, 79]. After this indentation the molecules may have rotated [80], but remain intact as can be inferred from their electronic resonance structure in the dI/dV–V spectra.

If larger bias voltages are used instead during the tip approach a dramatic change takes place in the molecular junction: a sudden drop in the current, as shown in figure 13, reveals an irreversible process. STM images taken afterward (see, e.g., the inset in figure 14) reveal an apparent deformation of the molecular structure. Typically, the molecules now appear more than 1 Å lower than their intact neighbor molecules. Most significative is the disappearance of the molecular resonances in the dI/dV–V spectra in figure 14. This strongly suggests that the icosahedral fullerene cage has been fragmented due to the large current density reached, and the molecule dissociated.

The fragmentation process takes place, for a fixed value of sample bias, around a specific threshold tunneling current. The way in which the cage rupture takes place may vary from one event to another, as the resulting features in the STM images are different. It should be noted that only the molecule directly underneath the tip is affected by the indentations. Neighboring molecules remain in their original states. We can thus exclude a polymerization with neighboring molecules [81]. We can also exclude a mechanical cracking of the cage by the STM tip: first, because at low bias voltages the tip can be indented far beyond the point of mechanical contact without apparent effect on the molecular integrity; second, because for large bias voltages the sudden drop in current is found already before a tip–molecule mechanical contact is formed (see figure 13(b)). It is then plausible that the decomposition of the fullerene's cage is a current-induced process. Rather than dealing with a current-induced dissociation of one C–C bond, as shown for smaller molecules [82, 83], the large current densities employed suggest that we are in the regime of vibrational heating of the fullerene, through the electron scattering and excitation of a set of cage vibrations. It is known that C_{60} can be thermally decomposed at temperatures around 1000 K [84–87]. Hence, energy accumulation in the fullerene, in the form of hot molecular vibrations, can be associated with an effective internal temperature that eventually is high enough to lead to the thermal-like fragmentation.

As a current-driven process, the fullerene fragmentation shows an intriguing dependence on the sample bias applied during the tip approach. We thus analyze the threshold current for molecular decomposition, I_{dec}, as a function of bias voltage. The threshold current is determined from the sudden drop in the I–z curves, I_{dec}, as well as the corresponding tip position z_{dec}. The statistical analysis of more than 180 molecules, given in figure 15(a), shows that both I_{dec} and z_{dec} depend critically on the applied bias value. In particular, I_{dec} shows a monotonic increase as the bias voltage is reduced [10]: for a bias voltage of 3.0 V an electron current $I_{dec} = 7$ μA is sufficient to decompose the C_{60} molecule, while electron currents as high as 70 μA can flow through the molecular junction before its degradation at 0.6 V. A more detailed look into the plot in figure 15(a) reveals two different regimes for fragmentation: below ∼1.2 V I_{dec} shows a strong increase with the inverse of the bias, while at larger bias voltages I_{dec} varies more smoothly. This region can be further divided by two plateaus at ∼1.5 and ∼2.5 V.

These regimes become even more evident when we plot instead the corresponding power, P_{dec}, applied to the C_{60} junction at the point of its decomposition ($P_{dec} = I_{dec}V$): the degradation power spectrum (figure 15(b)). Below ∼1.2 V P_{dec} increases sharply up to more than 50 μW as the bias is reduced down to 0.6 V. Above ∼1.2 V P_{dec} oscillates around a constant value of ∼21 μW, corresponding to the plateaus observed in the I_{dec} plot.

A first hint at the origin of the oscillations can be extracted when noting that the oscillations in the power spectrum match the energy alignment of the molecular resonances, sketched in the background of figure 15. When

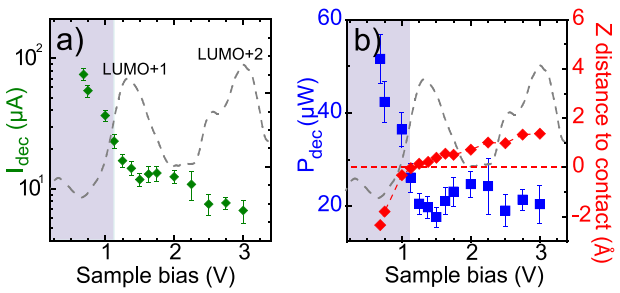

Figure 15. Degradation spectrum of C_{60} molecules on Cu(100). (a) Statistical average (of 180 molecules) of the current reached at the point of C_{60} degradation, I_{dec}, versus sample bias, V. Two sigma error vertical bars are indicated. (b) Bias dependence of the power applied at the point of degradation, $P_{dec} = I_{dec}V$ (left scale), and tip position with respect to the tip–molecule contact point (right scale). For degradation events occurring before the formation of a contact, the remaining distance to contact is obtained by a linear extrapolation. The blue shaded area indicates the regime where the decomposition takes place when the tip is in mechanical contact with the molecule. Reproduced with permission from [10]. Copyright 2008 American Physical Society.

a molecular resonance enters in the energy range of electron transport, the decomposition current and power are reduced. As described in section 3, the alignment of the molecular resonances of C_{60} depends on the substrate. To corroborate the correlation between the decomposition power and the resonance structure, we investigate the decomposition properties on different surfaces. In figure 16 we show the degradation power spectrum in comparison with the corresponding molecular resonance structure of C_{60} on Cu(110), Pb(111) and Au(111). In all three cases, we find a similar tendency: the power for molecular dissociation, P_{dec}, decreases when a new resonance enters the transport energy window. This qualitative behavior is explained by considering that a more efficient vibrational excitation takes place when the tunneling processes gain resonant character, in agreement with the results of section 4.1.2 [74, 88].

Theoretically, the temperature corresponding to the energy stored in the molecule can be computed. To simulate our data for dissociation of C_{60} on Cu(110), Pecchia *et al* modeled the electron transport by the non-equilibrium Green's function (NEGF) formalism [89]. In particular, they calculated the temperature for C_{60} on Cu(110) at different tip–sample distances. As can be deduced from figure 17(a), the temperature of C_{60} already reaches 1000 K before the LUMO resonance participates in the transport. Such high temperatures are reached with only a small fraction of electrons being inelastically scattered by molecular vibrations (10^{-3}). The temperature rises significantly further when the LUMO participates in the electron transport; in particular, the heating is largest when all C_{60} vibrational modes (all lying in a bandwidth of 200 meV above the resonance) can be excited.

A similar rise in molecular temperature appears at bias values where higher order resonances enter into the conduction. Curiously, at energies below the entrance of a resonance the heating is reduced. The origin of this is that tunneling electrons are able to absorb the energy of a hot vibration and tunnel resonantly through the state above. This

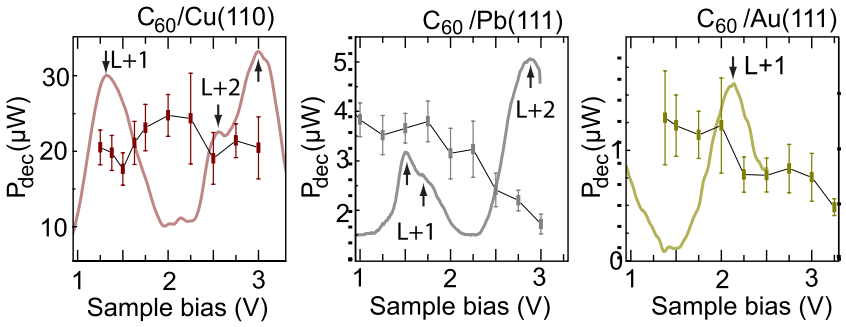

Figure 16. (a) Comparison of the degradation power spectra of C_{60} molecules on different substrates shown with their unoccupied resonant structures as obtained in STS spectra like those in figure 3. Arrows and letters identify the molecular states (L = LUMO). Reproduced with permission from [108]. Copyright 2011 Pan Stanford Publishing.

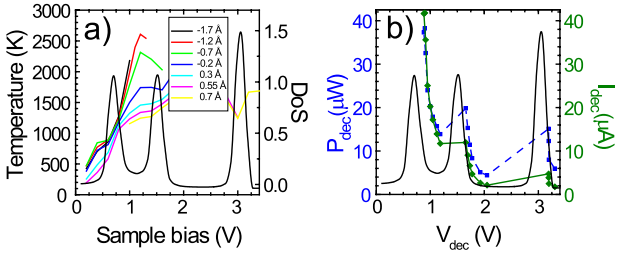

Figure 17. (a) Results of theoretical simulations of the molecular temperature as a function of the bias V applied between a Cu(110) surface and a single atom tip. (b) The values I_{dec} (diamonds, continuous line) and P_{dec} (squares, dark broken line) are marked for a threshold temperature of 1650 K for the C_{60} molecule. The black lines mark the molecular resonances as obtained from the simulations. Reproduced with permission from [10]. Copyright 2008 American Physical Society.

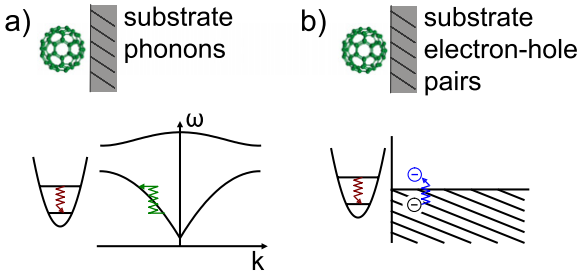

Figure 18. Scheme of the mechanisms of molecular vibration decay into excitations of the cold metal substrate: (a) decay into the metal phonon band and (b) creation of excited metal electrons (electron–hole pairs).

cooling mechanism can be very effective and, eventually, causes a lower rise of molecular temperature with bias voltage for sample biases right below a resonance level.

In the experiments, this resonant increase in molecular heating manifests itself as a decrease in the decomposition power. The resonant cooling translates into plateaus in I_{dec} and increase in P_{dec} at bias values below the corresponding resonance energy. A direct comparison between theory and experiment can be drawn by setting a critical decomposition temperature in the simulations. For $T_{dec} \sim 1650$ K the deduced values of I_{dec} and P_{dec} are shown in figure 17(b). The applied power follows the same trend of the molecules being less stable when more resonances carry the electron current.

6.2. Balance of excitations of molecular vibrations and their quenching into the leads

While the previous section showed the resonant character of molecular heating, this does not explain the large stability of C_{60} at bias voltages below 1.2 V. It should be noted that below this value the tip is in contact with the fullerene when the decomposition occurs. Another unsolved detail in the model of resonant heating is the significant difference in the total decomposition power for fullerenes on different surfaces. Figure 16 shows that the average power applied for degradation amounts to $\bar{P}_{dec} \sim 21$ μW for Cu(110), $\bar{P}_{dec} \sim 2.9$ μW for Pb(111), and $\bar{P}_{dec} \sim 1$ μW for Au(111).

To fully understand the decomposition properties, we need to consider the total vibrational energy stored in the molecule (and hence its model temperature). This depends on the balance between the heat generated by the inelastic scattering of electrons with molecular modes, and the heat dissipation into the 'cold' leads ($T = 5$ K) [74, 89, 90]. While the heat generation crucially depends on the coupling of electrons with molecular vibrations, its dissipation away from the molecular junction is determined by the coupling of these hot vibrations with the continuum of electrode excitations. Both generation and dissipation are important in determining the vibrational temperature reached by the molecule.

The important role of molecular cooling by relaxation of the molecular vibrations manifests itself in the large decomposition power needed for molecular dissociation when the tip is in contact with the molecule (figure 15). In this regime the equilibrium temperature is lower than that at the same electronic power when the tip is far away from the molecule. The presence of a good tip–molecule contact opens a second cooling channel for vibrations into the second metal electrode. Hence, the resulting temperature is significantly lower.

Possible mechanisms for relaxing the vibrational energy into the substrate are sketched in figure 18. One relaxation path is by damping the energy into the phonon modes of the substrate. However, this mechanism is not very efficient.

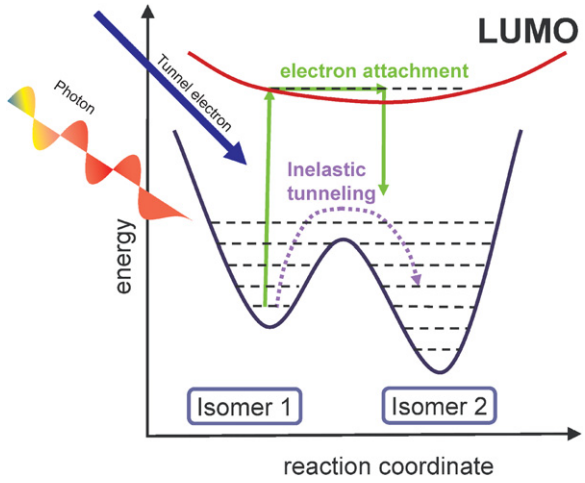

Figure 19. Schematic energy diagram of molecular switches, where two isomeric ground states are separated by an energy barrier. Switching between these low-energy states can be induced by light, electron attachment into the LUMO or multi-vibrational excitations.

The phonon band widths of the employed substrates are rather narrow. The phonon band width is largest for Cu(110) with a 42 meV width. For Pb(111) it is only 14 meV wide [91] and for Au(111) it is 16 meV [92]. On the other hand, the vibrational eigenenergies of C_{60} lie in a range between 33 and 200 meV. Hence, substrate phonons can only couple to external molecular vibrations of the fullerene with respect to the surface, which do not contribute to the thermal decomposition of the fullerene cage.

The more efficient mechanism for quenching of molecular vibrations is by excitation of electron–hole (e–h) pairs in the metallic substrates (figure 18(b)) [93]. One may expect that the efficiency of the e–h pair creation depends on the substrate's density of states (DoS) close to E_F. We test this assumption by comparing the DoSs of Cu(110), Pb(111), and Au(111) with the experimentally observed cooling rates as deduced from the decomposition powers on these surfaces. Comparison of the DoSs suggests that e–h pair creation is favored on Cu(110) with respect to the gold surface[1]. This would agree with our observations. However, this mechanism fails to explain the intermediate $\bar{P}_{dec}$ value found for degradation of C_{60} on Pb(111), since this metal surface has no surface state, and its density of bulk states at E_F is also the lowest of all three metals (see footnote 1).

The efficiency of e–h pair creation thus does not only depend on the substrate DoS. Considering the combined system of C_{60} and substrate, one finds a modified electronic structure close to E_F. As one can infer from the proximity and weight of the LUMO at E_F in figure 3, the adsorption of C_{60} leads to different amounts of charge transfer into the fullerene. There is hardly any charge transfer on Au(111), while there is some on Pb(111) and most on Cu(110). This sequence equals the one found for the stability of the C_{60} molecules. Hence, a large density of molecular states at E_F favors the creation of e–h pairs at the molecule, which are then coupled to the electronic bath of the substrate [6]. While additional effects like hybridization of metal and molecule electronic states may also play a role, our results suggest that charging a single molecule in contact with a metal electrode can help to sustain larger current densities passing through a single molecule.

[1] The densities of surface states are approximately 0.017 (eV Å^2)$^{-1}$ and 0.0105 (eV Å^2)$^{-1}$ for Cu(110) and Au(111) respectively [109–111]. The bulk DOSs at E_F are $DOS_{Pb}(E_F) = 0.0166$ (eV Å^3)$^{-1}$, $DOS_{Au}(E_F) = 0.0173$ (eV Å^3)$^{-1}$, $DOS_{Cu}(E_F) = 0.025$ (eV Å^3)$^{-1}$ [112].

7. Conclusions and outlook

Using the example of C_{60} we have observed fingerprints of molecular vibrations excited by electrons in a wide range of transport regimes: we have compared and characterized inelastic signals (i) in resonant and non-resonant transport; (ii) in the tunnel and contact regimes; and (iii) at small and large electron tunneling rates compared to the timescales of vibrational relaxations.

Electrons passing through single molecules may excite vibrations once the threshold energy of the eigenmode is reached. We were able to show that the efficiency of electron–vibration coupling largely depends on the degree of resonance character of the transport [44]. In conventional non-resonant IETS experiments the small tail of the LUMO thus enhances the probability of vibrational excitations. When the electrons have energies larger than the separation of the LUMO from E_F the transport process is fully resonant. In this case, the transported electrons occupy transient ionic vibronic states, which contribute as peaks in the dI/dV–V spectra. In principle this should lead to an even stronger vibrational signal. However, this is only detectable if the energy resolution is larger than the separation of the vibronic peaks [71]. The typical energy broadening of electronic states of molecules adsorbed on metal surfaces is >300 meV due to hybridization with substrate states and the short lifetimes of excited states. Hence, access to vibronic states in the resonant limit of electron transport can only be obtained by decreasing the electronic coupling of the molecule with the substrate.

When the rate of electrons inducing vibrations is larger than the vibrational relaxation rate, the molecule accumulates energy and gets hot. We were able to show that this energy suffices to thermally decompose C_{60} molecules. More importantly, we could show from the necessary decomposition power P_{dec} that the heating is more efficient in resonant transport conditions, in agreement with a larger electron–vibration coupling [10]. Furthermore, we could deduce trends in the relaxation rates of vibrations on metallic surfaces. Charge transfer into the organic molecule provides an enhanced DoS close to E_F. This facilitates the creation of e–h pairs, which accounts for the most prominent quenching pathway of molecular vibrations on metallic surfaces [11].

With this knowledge, one may envision strategies to use vibrations for chemical reactions of single molecules and, in particular, molecular switching processes. In a molecular switch, two isomeric states are separated by an energy barrier. It is a challenge to understand the potential energy diagrams of molecules adsorbed on a surface, which can deviate considerably from their counterparts in gas phase

or solution [94, 95], and to induce reversible switching [8, 42, 96–102]. A common approach is excitation by light [8, 98]. The photoexcited state of the molecule may relax into the other isomeric state. Alternatively, electrons from the tip of an STM can be used. The switching may take place in the ionic state by the attachment/detachment of an electron to the LUMO/from the HOMO [9]. Furthermore, the electric field in the STM junction may help in the isomerization process [96, 103]. The switching barrier can also be overcome by inelastically tunneling electrons. A combination of different modes as well as multiple excitations of the same mode can cause a transition from one side of the potential well to the other (see schematic in figure 19) [42, 100].

The distinction of the different electron-induced mechanisms requires a detailed analysis of the voltage and current dependence of the switching yield. The importance of certain vibrational modes can be unraveled by the electron–vibration coupling strength as observed in inelastic tunneling spectra. This is of particular interest if a combination of eigenmodes triggers the chemical reaction [82]. As we have seen in sections 4.1.2 and 6.1, a resonant character of the transport considerably enhances the excitation probability and therefore the switching yield. One may thus envision strategies to tune the energy level alignment by choosing an adequate molecule–substrate system.

One problem in the switching dynamics of molecules contacted to metal electrodes is the short lifetime of the electronically excited states. The rapid decay reduces the probability of transformation into the isomeric counterpart, since the time evolution in the electronically excited state is limited. An increase of the excited state's lifetime is possible by electronic decoupling of the switch from the surface either by inclusion of spacer layers as in section 5.1 [104] or by spacer legs directly attached to the molecular switch [8, 96, 98, 105, 106]. On the other hand, a fast cooling of the molecule is necessary to ensure the thermal stability of the molecule during electron transport (section 6). Hence, design strategies have to find the right balance between switching capabilities and device stability.

Acknowledgments

We are indebted to G Schulze for great contributions and stimulating discussions throughout the whole work. We thank A Arnau, T Frauenheim, T Frederiksen, A Gagliardi, N Lorente, T Niehaus, and A Pecchia for fruitful theoretical collaborations. We gratefully acknowledge the financial support from the Deutsche Forschungsgemeinschaft through the collaborative research center Sfb658 'Elementary processes in molecular switches at surfaces' and SPP1243 'Quantum transport at the molecular scale'.

References

[1] Galperin M, Ratner M A and Nitzan A 2007 *J. Phys.: Condens. Matter* **19** 103201
[2] Stipe B C, Rezaei M A and Ho W 1998 *Science* **280** 1732
[3] Ho W 2002 *J. Chem. Phys.* **117** 11033
[4] Qiu X H, Nazin G V and Ho W 2004 *Phys. Rev. Lett.* **92** 206102
[5] Liu N, Pradhan N A and Ho W 2004 *J. Chem. Phys.* **120** 11371
[6] Persson M and Hellsing B 1982 *Phys. Rev. Lett.* **49** 662
[7] Dulic D, van der Molen S J, Kudernac T, Jonkman H T, de Jong J J D, Bowden T N, van Esch J, Feringa B L and van Wees B J 2003 *Phys. Rev. Lett.* **91** 207402
[8] Comstock M J *et al* 2007 *Phys. Rev. Lett.* **99** 038301
[9] Bronner C, Schulze G, Franke K J, Pascual J I and Tegeder P 2011 *J. Phys.: Condens. Matter* **23** 484005
[10] Schulze G *et al* 2008 *Phys. Rev. Lett.* **100** 136801
[11] Schulze G, Franke K J and Pascual J I 2008 *New J. Phys.* **10** 065005
[12] Chancey C C and O'Brien M C M 1997 *The Jahn–Teller Effect in C_{60} and Other Icosahedral Complexes* (Princeton, NJ: Princeton University Press)
[13] Menendez J and Page J B 2000 *Light Scattering in Solids VIII* ed M Cardona and G Güntherodt (Berlin: Springer)
[14] Gunnarsson O *et al* 1995 *Phys. Rev. Lett.* **74** 1875
[15] Cavar E, Blum M-C, Pivetta M, Patthey F, Cherqui M and Schneider W-D 2005 *Phys. Rev. Lett.* **95** 196102
[16] Pradhan N A, Liu N and Ho W 2005 *J. Phys. Chem.* B **109** 8513
[17] Pascual J I, Gomez-Herrero J, Sanchez-Portal D and Rust H-P 2002 *J. Chem. Phys.* **117** 9531
[18] Grobis M, Khoo K H, Yamachika R, Lu X, Nagaoka K, Louie S G, Crommie M F, Kato H and Shinohara H 2005 *Phys. Rev. Lett.* **94** 136802
[19] Parks J J, Champagne A R, Hutchison G R, Flores-Torres S, Abruna H D and Ralph D C 2007 *Phys. Rev. Lett.* **99** 026601
[20] Bohler T, Edtbauer A and Scheer E 2007 *Phys. Rev.* B **76** 125432
[21] Rogero C, Pascual J I, Gomez-Herrero J and Baro A M 2002 *J. Chem. Phys.* **116** 832
[22] Grobis M, Lu X and Crommie M F 2002 *Phys. Rev.* B **66** 161408
[23] Lu X, Grobis M, Khoo K H, Louie Steven G and Crommie M F 2003 *Phys. Rev. Lett.* **90** 096802
[24] Silien C, Pradhan N A, Thiry P A and Ho W 2004 *Phys. Rev.* B **69** 115434
[25] Schull G and Berndt R 2007 *Phys. Rev. Lett.* **99** 226105
[26] Schull G, Dappe Y J, Gonzalez C, Bulou H and Berndt R 2011 *Nano Lett.* **11** 3142
[27] Fasel R *et al* 1999 *Phys. Rev.* B **60** 4517
[28] Li H, Franke K J, Pascual J I, Bruch L W and Diehl R D 2009 *Phys. Rev.* B **80** 085415
[29] Lu X, Grobis M, Khoo K H, Louie S G and Crommie M F 2004 *Phys. Rev.* B **70** 115418
[30] Jacklevic R C and Lambe J 1966 *Phys. Rev. Lett.* **17** 1139
[31] Komeda T 2005 *Prog. Surf. Sci.* **78** 41
[32] Lorente N, Persson M, Lauhon L J and Ho W 2001 *Phys. Rev. Lett.* **86** 2593
[33] Troisi A and Ratner M A 2006 *Nano Lett.* **6** 1784
[34] Paulsson M, Frederiksen T, Ueba H, Lorente N and Brandbyge M 2008 *Phys. Rev. Lett.* **100** 226604
[35] Garcia-Lekue A, Sanchez-Portal D, Arnau A and Frederiksen T 2011 *Phys. Rev.* B **83** 155417
[36] Stipe B C, Rezaei M A and Ho W 1998 *Science* **279** 1907
[37] Stipe B C, Rezaei M A, Ho W, Gao S, Persson M and Lundqvist B I 1997 *Phys. Rev. Lett.* **78** 4410
[38] Komeda T, Kim Y, Kawai M, Persson B N J and Ueba H 2002 *Science* **295** 2055
[39] Kim Y, Komeda T and Kawai M 2002 *Phys. Rev. Lett.* **89** 126104
[40] Pascual J I, Lorente N, Song Z, Conrad H and Rust H P 2003 *Nature* **423** 525

[41] Sainoo Y, Kim Y, Okawa T, Komeda T, Shigekawa H and Kawai M 2005 *Phys. Rev. Lett.* **95** 246102
[42] Henzl J, Mehlhorn M, Gawronski H, Rieder K-H and Morgenstern K 2006 *Angew. Chem. Int. Edn* **45** 603
[43] Motobayashi K, Kim Y, Ueba H and Kawai M 2010 *Phys. Rev. Lett.* **105** 076101
[44] Franke K J, Schulze G and Pascual J I 2010 *J. Phys. Chem. Lett.* **1** 500
[45] Sergueev N, Demkov A A and Guo H 2007 *Phys. Rev.* B **75** 233418
[46] Fang Y, Huang Q-J, Wang P, Li X-Y and Yu N-T 2003 *Chem. Phys. Lett.* **381** 255
[47] Okabayashi N, Konda Y and Komeda T 2008 *Phys. Rev. Lett.* **100** 217801
[48] Persson B N J and Baratoff A 1987 *Phys. Rev. Lett.* **59** 339
[49] Mingo N and Makoshi K 2000 *Phys. Rev. Lett.* **84** 3694
[50] Lorente N and Persson M 2000 *Phys. Rev. Lett.* **85** 2997
[51] Hahn J R, Lee H J and Ho W 2000 *Phys. Rev. Lett.* **85** 1914
[52] Persson B N J and Persson M 1980 *Solid State Commun.* **36** 175
[53] Smit R H M, Noat Y, Untiedt C, Lang N D, van Hemert M C and van Ruitenbeek J M 2002 *Nature* **419** 906
[54] Agrait N, Untiedt C, Rubio-Bollinger G and Vieira S 2002 *Chem. Phys.* **281** 231
[55] Tal O, Krieger M, Leerink B and van Ruitenbeek J M 2008 *Phys. Rev. Lett.* **100** 196804
[56] Neel N, Kröger J, Limot L, Frederiksen T, Brandbyge M and Berndt R 2007 *Phys. Rev. Lett.* **98** 065502
[57] Scheer E, Joyez P, Esteve D, Urbina C and Devoret M H 1997 *Phys. Rev. Lett.* **78** 3535
[58] Kröger J, Neel N and Limot L 2008 *J. Phys.: Condens. Matter* **20** 223001
[59] Neel N, Kröger J and Berndt R 2011 *Nano Lett.* **11** 3593
[60] Vitali L, Ohmann R, Kern K, Garcia-Lekue A, Frederiksen T, Sanchez-Portal D and Arnau A 2010 *Nano Lett.* **10** 657
[61] Repp J, Meyer G, Paavilainen S, Olsson F E and Persson M 2005 *Phys. Rev. Lett.* **95** 225503
[62] Qiu X H, Nazin G V and Ho W 2003 *Science* **299** 542
[63] Nilius N, Wallis T M and Ho W 2003 *Phys. Rev. Lett.* **90** 046808
[64] Heinrich A J, Gupta J A, Lutz C P and Eigler D M 2004 *Science* **306** 466
[65] Repp J, Meyer G, Stojkovic S M, Gourdon A and Joachim C 2005 *Phys. Rev. Lett.* **94** 026803
[66] Hirjibehedin C F, Lutz C P and Heinrich A J 2006 *Science* **312** 1021
[67] Loth S, Etzkorn M, Lutz C P, Eigler D M and Heinrich A J 2010 *Science* **329** 1628
[68] Zhao J, Zeng C, Cheng X, Wang K, Wang G, Yang J, Hou J G and Zhu Q 2005 *Phys. Rev. Lett.* **95** 045502
[69] Li B, Zeng C, Zhao J, Yang J, Hou J G and Zhu Q 2006 *J. Chem. Phys.* **124** 064709
[70] Nazin G V, Wu S W and Ho W 2005 *Proc. Natl Acad. Sci.* **102** 8832
[71] Frederiksen T, Franke K J, Arnau A, Schulze G, Pascual J I and Lorente N 2008 *Phys. Rev.* B **78** 233401
[72] Franke K J, Schulze G, Henningsen N, Fernandez-Torrente I, Pascual J I, Zarwell S, Rück-Braun K, Cobian M and Lorente N 2008 *Phys. Rev. Lett.* **100** 036807
[73] Fernandez-Torrente I, Franke K J and Pascual J I 2008 *J. Phys.: Condens. Matter* **20** 184001
[74] Galperin M, Ratner M A and Nitzan A 2007 *J. Phys.: Condens. Matter* **19** 103201
[75] Galperin M, Nitzan A and Ratner M A 2007 *Phys. Rev.* B **76** 035301
[76] Huang Z *et al* 2006 *Nano Lett.* **6** 1240
[77] Huang Z *et al* 2007 *Nature Nanotechnol.* **2** 698
[78] Tour J M 2000 *Acc. Chem. Res.* **33** 791
[79] Joachim C, Gimzewski J K, Schlittler R R and Chavy C 1995 *Phys. Rev. Lett.* **74** 2102
[80] Néel N, Limot L, Kröger J and Berndt R 2008 *Phys. Rev.* B **77** 125431
[81] Zhao Y B *et al* 1994 *Appl. Phys. Lett.* **64** 577
[82] Simic-Milosevic V, Mehlhorn M, Rieder K-H, Meyer J and Morgenstern K 2007 *Phys. Rev. Lett.* **98** 116102
[83] Sakulsermsuk S, Sloan P A and Palmer R E 2010 *ACS Nano* **4** 7344
[84] Cepek C, Goldoni A and Modesti S 1996 *Phys. Rev.* B **53** 7466
[85] Pascual J I, Gomez-Herrero J and Baro A M 1998 *Surf. Sci.* **397** L267
[86] Swami N, He H and Koel B E 1999 *Phys. Rev.* B **59** 8283
[87] Saltas V and Papageorgopoulos C A 2001 *Surf. Sci.* **488** 23
[88] Galperin M, Nitzan A and Ratner M A 2007 *Phys. Rev.* B **75** 155312
[89] Pecchia A, Romano G and Di Carlo A 2007 *Phys. Rev.* B **75** 035401
[90] Romano G, Pecchia A and Di Carlo A 2007 *J. Phys.: Condens. Matter* **19** 215207
[91] Fuhrmann D and Wöll C 1996 *Surf. Sci.* **368** 20
[92] Wang X Q 1991 *Phys. Rev. Lett.* **67** 1294
[93] Gao S, Persson M and Lundqvist B I 1992 *Solid State Commun.* **84** 271
[94] Piantek M *et al* 2009 *J. Am. Chem. Soc.* **131** 12729
[95] Mielke J, Leyssner F, Koch M, Meyer S, Luo Y, Selvanathan S, Haag R, Tegeder P and Grill L 2011 *ACS Nano* **5** 2090
[96] Alemani M, Peters M V, Hecht S, Rieder K-H, Moresco F and Grill L 2006 *J. Am. Chem. Soc.* **128** 14446
[97] Choi B-Y, Kahng S-J, Kim S, Kim H, Kim H W, Song Y J, Ihm J and Kuk Y 2006 *Phys. Rev. Lett.* **96** 156106
[98] Hagen S, Leyssner F, Nandi D, Wolf M and Tegeder P 2007 *Chem. Phys. Lett.* **444** 85
[99] Liljeroth P, Repp J and Meyer G 2007 *Science* **317** 1203
[100] Nacci C, Fölsch S, Zenlchowski K, Dokic J, Klamroth T and Saalfrank P 2009 *Nano Lett.* **9** 2996
[101] van der Molen S J and Liljeroth P 2010 *J. Phys.: Condens. Matter* **22** 133001
[102] Pechenezhskiy I V, Cho J, Nguyen G D, Berbil-Bautista L, Giles B L, Poulsen D A, Frechet J M J and Crommie M F 2012 *J. Phys. Chem.* C **116** 1052
[103] Henningsen N, Franke K J, Torrente I F, Schulze G, Priewisch B, Rück-Braun K, Dokic J, Klamroth T, Saalfrank P and Pascual J I 2007 *J. Phys. Chem.* C **111** 14843
[104] Safiei A, Henzl J and Morgenstern K 2010 *Phys. Rev. Lett.* **104** 216102
[105] Wolf M and Tegeder P 2009 *Surf. Sci.* **603** 1506
[106] McNellis E R, Mercurio G, Hagen S, Leyssner F, Meyer J, Soubatch S, Wolf M, Reuter K, Tegeder P and Tautz F S 2010 *Chem. Phys. Lett.* **499** 247
[107] Horcas I *et al* 2007 *Rev. Sci. Instrum.* **78** 013705
[108] Schulze G, Franke K J and Pascual J I 2011 *Current-Driven Phenomena in Nanoelectronics* ed T Seideman (Singapore: Pan Stanford)
[109] Kevan S 1983 *Phys. Rev.* B **28** 4822
[110] Aebi P, Osterwalder J, Fasel R, Naumović D and Schlapbach L 1994 *Surf. Sci.* **307–309** 917
[111] LaShell S, McDougall B A and Jensen E 1996 *Phys. Rev. Lett.* **77** 3419
[112] Papaconstantopoulos D A 1986 *Handbook of the Band Structure of Elemental Solids* (New York: Plenum)